Understanding the nano- and macromechanical behaviour, the failure and fatigue mechanisms of advanced and natural polymer fibres by Raman/IR microspectrometry

Philippe Colomban

▶ **To cite this version:**

Philippe Colomban. Understanding the nano- and macromechanical behaviour, the failure and fatigue mechanisms of advanced and natural polymer fibres by Raman/IR microspectrometry. Advances in Natural Sciences : Nanoscience and Nanotechnology, 2013, 4 (1), pp.013001. 10.1088/2043-6262/4/1/013001 . hal-01542272

HAL Id: hal-01542272

https://hal.sorbonne-universite.fr/hal-01542272

Submitted on 19 Jun 2017

HAL is a multi-disciplinary open access archive for the deposit and dissemination of scientific research documents, whether they are published or not. The documents may come from teaching and research institutions in France or abroad, or from public or private research centers.

L'archive ouverte pluridisciplinaire **HAL**, est destinée au dépôt et à la diffusion de documents scientifiques de niveau recherche, publiés ou non, émanant des établissements d'enseignement et de recherche français ou étrangers, des laboratoires publics ou privés.

Distributed under a Creative Commons Attribution 4.0 International License

IOPscience iopscience.iop.org

Home Search Collections Journals About Contact us My IOPscience

Understanding the nano- and macromechanical behaviour, the failure and fatigue mechanisms of advanced and natural polymer fibres by Raman/IR microspectrometry

This content has been downloaded from IOPscience. Please scroll down to see the full text.

2013 Adv. Nat. Sci: Nanosci. Nanotechnol. 4 013001

(http://iopscience.iop.org/2043-6262/4/1/013001)

View the table of contents for this issue, or go to the journal homepage for more

Download details:

IP Address: 134.157.80.157
This content was downloaded on 19/06/2017 at 14:41

Please note that terms and conditions apply.

You may also be interested in:

In situ high pressure and high temperature Raman studies of (1-x)SiO2xGeO2glasses
R Le Parc, V Ranieri, J Haines et al.

Physical characterization of functionalized spider silk: electronic and sensing properties
Eden Steven, Jin Gyu Park, Anant Paravastu et al.

Nanomechanics of silk: the fundamentals of a strong, tough and versatile material
Isabelle Su and Markus J Buehler

Optimization of the silk scaffold sericin removal process
Thomas K H Teh, Siew-Lok Toh and James C H Goh

Drug loading and release on tumor cells using silk fibroin–albumin nanoparticles as carriers
B Subia and S C Kundu

Deformation of isolated single-wall carbon nanotubes in electrospun polymernanofibres
Prabhakaran Kannan, Stephen J Eichhorn and Robert J Young

Load transfer and mechanical properties of chemically reduced graphene reinforcements in polymer composites
Peng Xu, James Loomis, Roger D Bradshaw et al.

Transparent and flexible resistive switching memory devices with a very high ON/OFF ratio using gold nanoparticles embedded in a silk protein matrix
Narendar Gogurla, Suvra P Mondal, Arun K Sinha et al.

Biomaterials in light amplification
Jaroslaw Mysliwiec, Konrad Cyprych, Lech Sznitko et al.

OPEN ACCESS
IOP PUBLISHING
ADVANCES IN NATURAL SCIENCES: NANOSCIENCE AND NANOTECHNOLOGY
Adv. Nat. Sci.: Nanosci. Nanotechnol. **4** (2013) 013001 (10pp)
doi:10.1088/2043-6262/4/1/013001

REVIEW

Understanding the nano- and macromechanical behaviour, the failure and fatigue mechanisms of advanced and natural polymer fibres by Raman/IR microspectrometry*

Philippe Colomban[1,2]

[1] Laboratoire de Dynamique, Interaction et Réactivité (LADIR), Université Pierre-et-Marie Curie (UPMC), c49, 4 Place Jussieu, F-75252 Paris Cedex 05, France
[2] UMR 7075, CNRS, 4 Place Jussieu, F-75252 Paris Cedex 05, France

E-mail: philippe.colomban@upmc.fr

Received 11 October 2012
Accepted for publication 1 December 2012
Published 19 December 2012
Online at stacks.iop.org/ANSN/4/013001

Abstract
The coupled mechanical and Raman/infrared (IR) analysis of the (nano)structure and texture of synthetic and natural polymer fibres (polyamides (PA66), polyethylene terephthalate (PET), polypropylene (PP), poly(paraphenylene benzobisoxazole) (PBO), keratin/hair, *Bombyx mori*, *Gonometa rufobrunea/postica Antheraea/Tussah* silkworms and *Nephila Madagascarensis* spider silks) is applied so as to differentiate between crystalline and amorphous macromolecules. Bonding is very similar in the two cases but a broader distribution of conformations is observed for the amorphous macromolecules. These conclusions are then used to discuss the modifications induced by the application of a tensile or compressive stress, including the effects of fatigue. Detailed attention is paid to water and the inter-chain coupling for which the importance of hydrogen bonding is reconsidered. The significant role of the 'amorphous' bonds/domains in the process of fracture/fatigue is shown.

Keywords: mechanics, fibre, Raman, infrared, nanostructure

Classification numbers: 2.06, 4.00, 5.11

1. Introduction

Natural fibres have been used for millennia for textile and utensils (rope, cable, surgery etc), as-collected or after complex processing. As a function of the use, the highest strength or strain is researched; the combination of both leading to the best reliability because of the maximization of the work of fracture (the area delimited by the curve in figure 1). A variety of synthetic fibres, made of polymer or inorganic materials, were developed after the Second World War, some bio-sourced (e.g. rayonne/viscose and Rilsan^{TM} [1]), for very different applications, alone, woven or not, and as matrix reinforcement (composite materials). They exhibit a very high ultimate strength (up to 4–6 GPa) or a high strain (up to >50%) [2]. The combination of the mechanical properties and of the fibre diameter determines the possible curvature radius without fracture (note the matter of a curved fibre is submitted both to compression (internal radius side) and traction (external radius side)). Consequently,

* Invited talk at the 6th International Workshop on Advanced Materials Science and Nanotechnology IWAMSN2012, 30 October–2 November 2012, Ha Long, Vietnam.

© 2013 Vietnam Academy of Science & Technology

Original content from this work may be used under the terms of the Creative Commons Attribution 3.0 licence. Any further distribution of this work must maintain attribution to the author(s) and the title of the work, journal citation and DOI.

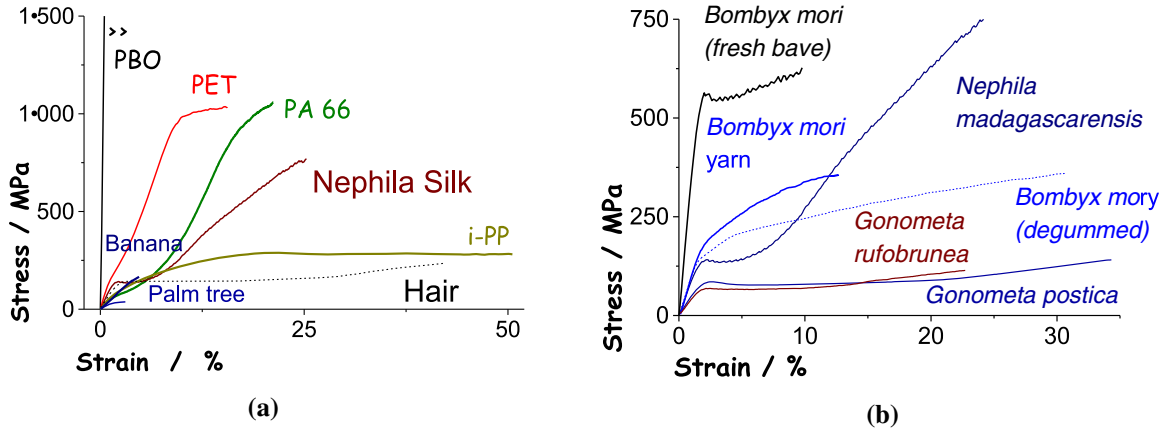

Figure 1. Representative tensile stress–strain curves measured for different synthetic (PBO, PET, PA66, i-PP (a)) and natural fibres: silk (*Bombyx, Nephila and Gonometa*), keratin (hair) and cellulose fibres (banana leaf, palm tree sheath (b)). The area delimited by the curve and the *x*-axis corresponds to the work to be dissipated before the fracture (see [8, 22]).

small diameter fibres are searched with diameter ranging between a few and a few tens of microns. Actually the behaviour of many fibres in compression and tension was not well known. It was not only the case for new systems such as, for example, the PBO (poly(paraphenylene benzobisoxazole) Zylon™ fibre exhibiting better properties than Kevlar™ (figure 1(a)) but also for 'older' systems such as polyamide fibres (Nylon™ and counterparts) or high performance natural fibres (animal—silkworm or spider silks, keratin or vegetal—hemp etc, figure 1(b)).

A very important characteristic of the mechanical properties is that they do not only depend on the matter, but also on the object: in a rough description, as a function of the 'quality' of the sample processing, it is more or less possible to explore the potential of the mechanical properties of the material. Consequently, a statistical approach is mandatory: for example, the ultimate strength of a fibre highly depends on the defect number at the origin of crack initiation; in contrast the Young's modulus, the slope of the stress–strain curve according to Hooke's model, is rather independent of the sample characteristics and considered to reflect relatively well the material properties. Basically, the mechanic behaviour of an object will depend on (i) the strength of the chemical bonds and the density of bonds per unit volume, (ii) the distribution and size of 'critical' defects and (iii) the applied load and the object history (processing and ageing) and the object/part dimensions. In many cases the sampling/measurement modifies the object and makes the extraction of reliable data and their comparison complex.

Vibrational spectroscopies, namely infrared absorption and Raman scattering, can be non-destructive and non-invasive, which allows coupling these methods with mechanical testing (*in operando* analysis). They probe the matter through mechanics (wavenumbers=vibrational eigenfrequencies) and the inter-atomic/molecular charge transfers (the peak intensity is either a direct (IR) or an indirect (Raman—requires multiplication by the frequency) measurement of conductivity [3]). Not only the position (wavenumber) but also the form (Lorentzian, Gaussian or more complex shape), the width and the polarization of the Raman and IR components gives valuable information on the composition (elongation modes are characteristic of the chemical bonds or molecular functions), the short-range to long-range structure (polarizations and collective low energy modes) and the texture (polarization and wavenumber mappings) of the fibres. The comparisons of polarized signatures for horizontal (H) and vertical (V) configurations obtained by changing the orientation of the fibre with respect to the laser and spectrometer slit entrance, is a good means for measuring the axial and/or crystalline character of the fibre [3–5].

On the basis of x-ray diffraction and macromolecular modelling, the polymer fibres are described as composed of 'domains' with variable crystallinity (crystallized, 'oriented amorphous' and 'amorphous' matter, figure 2). The distribution of these zones along the fibres and across their section (skin/core gradient) is unknown in the vast majority of the cases and subject to debate. However, common crystallographic descriptions that assume different degrees of crystallinity can be identified although it is not possible, or is at least difficult, to differentiate in the reciprocal space (where x-ray diffraction is performed) a progressive orientational disorder (the para-crystal model from Von Hoseman [6, 7]) from a juxtaposition of more or less ordered domains. The differentiation between the domains—or crystallite-size (according to the Scherrer formula [6])—and the coherence length is reasonable in metals, or in ionic compounds where substitution defects are numerous, but not necessarily in molecular compounds. It is indeed much easier, from an energetic point of view, to have a dihedral rotation around the chemical bond or even to deform covalent bond angles leading to an orientational disorder [8–10] than to modify the inter-atomic distances. These invariant distances cause the rare 'Bragg' peaks for corresponding (short!) inter-reticular distances (figure 2(a)). The continuous deformation the para-crystal model (i.e. without origin and borders) seems therefore more reasonable, although not much considered in the literature. In many fibres, inter-chain hydrogen bonds are assumed to form overlaps, crossings, loops etc (figure 3). It is supposed that these conditions, at the same time, control the performance of the fibre, in rigidity (tension of the molecular chains) and elasticity (disentanglement and tension of the chains of the amorphous zones) and in addition, the modes of fatigue and failure (initiation, propagation).

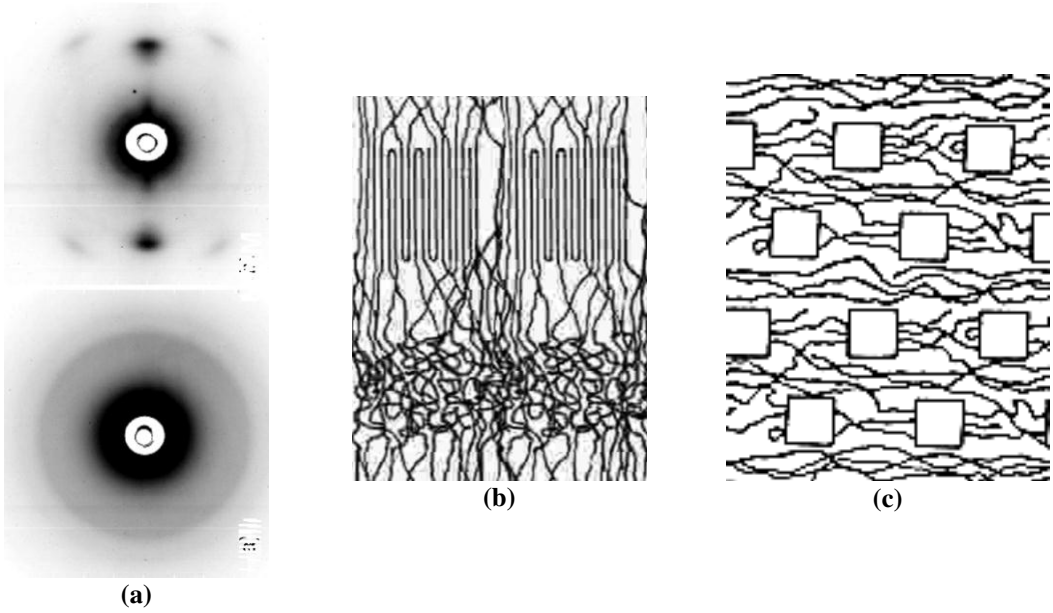

Figure 2. (a) Representative x-ray patterns measured for amorphous (bottom, dried silk *Bombyx mori* gland) and (poor) 'crystalline' (*Bombyx mori* fibre), (b) sketch showing macromolecular chains belonging to 'crystalline', oriented amorphous and amorphous areas (Prevorsek's model) and (c) crystalline islands in an amorphous polymer matrix (Oudet's model).

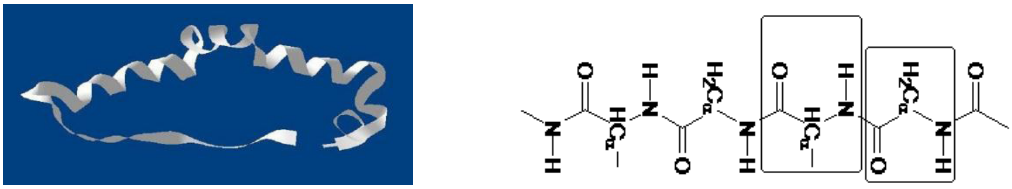

Figure 3. Sketch example (a) of Chem3D short-range structure of the spidroin macromolecule (spider silk [8]): see regular helix, helix defects and turns and untwisted ribbons available for β-sheet conformations. This illustrates the easy orientational disorder of polymer chain. Sketch of the polyamide silk macromolecule chain (b); boxes correspond to lysine and alanine, the most observed amino acid residues.

Complex processes of heating-extrusion–extension or spinning from a liquid state crystal regulate the texture of high-performance synthetic fibres. The mechanisms correlating texture and nano-/micro-properties remain to be clarified.

We will review the broad possibilities that Raman, and some extended IR-microspectrometry in combination with tensile/compressive solicitations offer in the study of the (nano)texture and the (nano)mechanical behaviour of fibres by closely analysing the spectra. Techniques of deuteration developed for the study of compounds with hydrogen bonding (protonic conductors in particular [11]) will be also deal with. We will take synthetic PA66 polyamide, polyethylene terephthalate (PET) and isotactic polypropylene (i-PP) fibres and 'natural' polyamide materials, namely silks and keratin (hair) fibres, as examples [12–21].

Actually most of the Raman studies of polymer materials are limited to the stretching mode domain, typically 1000–2000 cm^{-1} [23–25] and other spectral regions rarely considered [26–28]. An analysis of the whole spectrum allowed the selection of the most relevant probes: (i) low-wavenumber modes around 50–100 cm^{-1}, corresponding to collective movements ('lattice modes') and/or representing the shearing-friction of the macromolecule chains, very sensitive to the medium and long-range order, (ii) modes of νN–H isolated vibrators probing the first neighbouring shell by means of the inter/intra-chain hydrogen bond and (iii) amid I modes characterizing the chain modification (νC=O; νC–N). Although the latter modes have received considerable attention and are usually assigned to helix or β-sheet conformations, the other modes are generally ignored. The analysis in load (or strain)-controlled traction [7, 12–14, 16, 18] and hydrostatic compression (in a diamond anvil cell [15, 29]) clearly highlights different thresholds of tension/compression for 'crystalline/ordered' and 'amorphous/disordered' bonds, in agreement with the macroscopic mechanical analyses. We will also consider the differentiation of bonds belonging to an 'ordered' macromolecule/area from those pertaining to 'amorphous' ones by using the technique of isotopic dilution H/D [26].

2. Experimental

2.1. Samples

Synthetic and natural fibres are stored under controlled water partial pressure at room temperature. Some fibres are annealed at various temperatures or encapsulated with water (H_2O) or heavy water (D_2O) in long Pyrex tubes [29].

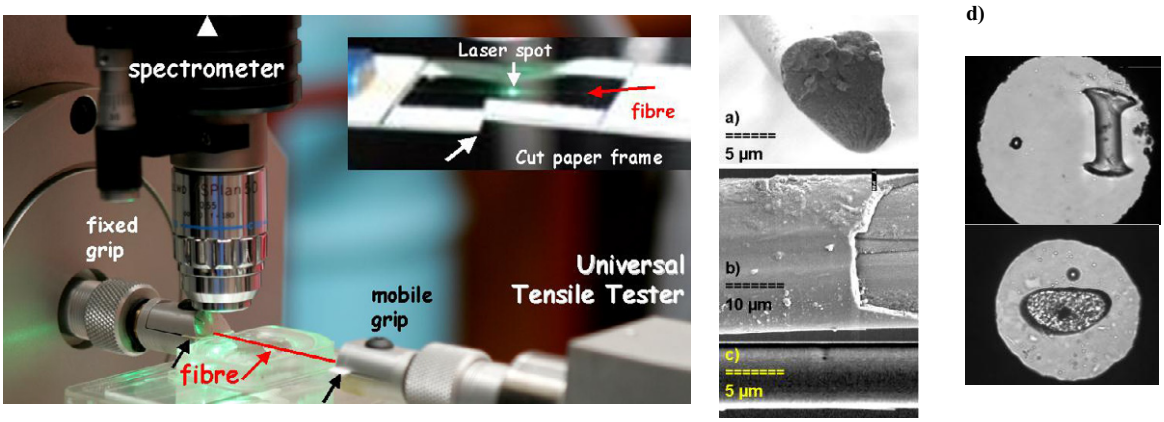

Figure 4. Detail of the Raman set-up for measurement of single fibre under controlled load or strain; the insert shows the laser focused on the fibre, the paper frame has been cut just before measurement. An SEM image of a fractured *Bombyx mori* section is shown (a); note the sericin sheath around the two fibres of a *Bombyx mori* bave (b) and the very clear, sericin-free *Nephila madagascarensis* spider fibre (c). Polyamide PA66 fibre piece and hair fibre section in the Diamond Anvil cell (cell diameter: 200 μm; note the small ruby ball for pressure calibration) (d).

Fresh hand-spun, cocoon extracted and aged silkworm/spider fibres were studied before (the bave consists of two fibres embedded in a common sericin sheath) and after degumming (see [8, 16–18] for details). Regenerated silk was studied either in the gel or in the dried film state (thickness 10–50 μm). The regenerated silk was also used to prepare silk fibre-reinforced regenerated silk-matrix composites [19, 30].

The fibres (diameter between ∼5 (spider silk) and ∼30 (PA66) μm) are cut either in pieces a few tens of micron long for study under hydrostatic pressure (figure 4(d)) or a few tens of mm for tensile studies (figure 4(a)). Fibre tips are taped onto gold-coated glass plates, or mounted on paper to be assembled in a universal tester as previously described [7, 16].

2.2. Tensile behaviour and Raman study under controlled stress/strain

The mechanical tensile properties of the samples were obtained using (computer controlled) Universal Fibre Testers (UFT) previously described [16]. The gauge length was 30 mm. The Tester was set under the ×50 or ×100 long working distance objective (total magnification ×500 or ×1000) of high resolution Raman spectrometers (figure 4, [7, 8]). The orientation of the fibre/tester versus the laser polarization was chosen to obtain the stronger signal.

2.3. Microspectrometries

The Raman spectra were recorded at controlled temperature with different spectrometers equipped with lasers delivering (514.5 or 532 nm) green or (785 nm) red lines. A motorized XY table makes it possible to carry out mapping with $a >$ 0.1 μm step. The laser power is controlled, typically <2 mW at the sample. A neon lamp is added to control the absolute wavenumber position [8].

A Lorentzian (L) shape for the 'crystalline/molecular' modes and a Gaussian (G) shape for the 'amorphous' signal are expected according to the Raman theory and the configuration distribution. Lab-developed software was used for the data extraction from the linescan/mapping hyperspectrum.

Measurements under hydrostatic pressure are taken through a diamond anvil cell, the pressure being calibrated with the fluorescence lines of chromium ions in ruby crystals [29]. The infrared microscope/ATR is an Equinox 55 Fourier transform Michelson interferometer with an ATR 'golden gate' input (Bruker, France). It is designed to examine the surface (a few microns in depth) of a material brought into 'perfect' contact with the ATR crystal. An Irscope II microscope with Cassegrain objectives makes it also possible to work in transmission for samples with thickness less than 30 μm. The spot diameter of ∼200 μm is reduced to 20 μm with a diaphragm, to separately analyse the core and the skin of a fibre.

3. Tensile measurements

First, the material and its history determine the mechanical behaviour. This is well known by engineers optimizing the mechanical properties of advanced fibres by the synthesis control and the combination of thermal and mechanical treatments. For instance the PBO fibre, a highly crystalline polymer chain built with aromatic cycles exhibits a huge Young's modulus and breaks at a very low strain level (<1%) but its ultimate strength is over 3 GPa (figure 1(a)). In contrast, the isotactic polypropylene fibre shows a great strain. Similar features are observed for natural fibres, for instance for keratin fibres (hair, wools etc). Figure 5 shows representative examples of the five different types of signatures that could be identified for natural polyamides. Note that some different stress–strain curve shapes have already been observed [31], but assigned as characteristic of the studied creature. For each series, whatever the creature, a large dispersion of the ultimate stress and strain was observed but five different stress versus strain curves could be distinguished unambiguously. Our attention was focused on silkworm and dragline spider fibres because these natural fibrous proteins appear the simplest case for a better understanding of this class of polymer materials.

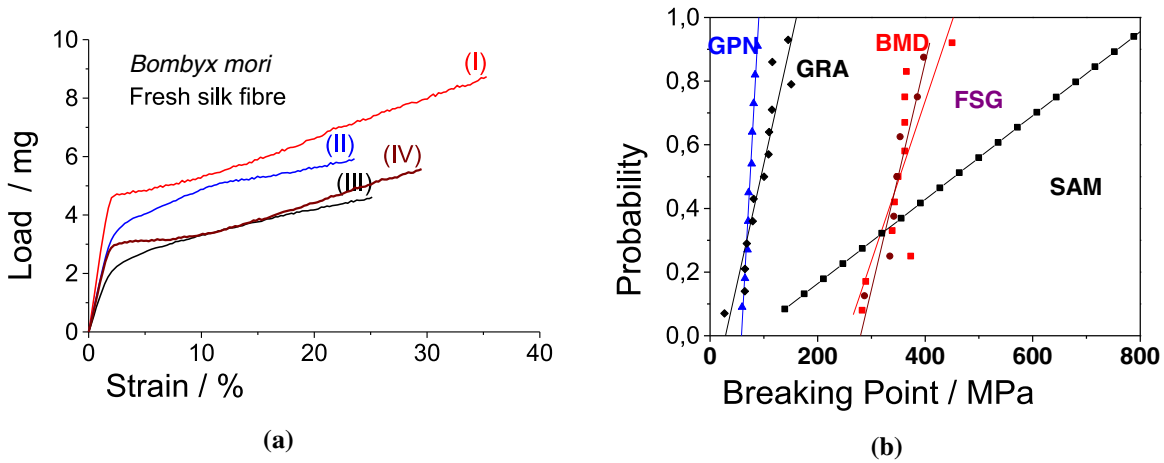

Figure 5. (a) Load(Stress) versus strain behaviours observed on fresh undegummed *Bombyx mori* fibres. (b) Weibull distribution of the ultimate tensile strength (a) for *Gonometa postica* (GPN), *Gonometa rufobrunea* (GRA), degummed *Bombyx mori* (BMD), undegummed yarn-extracted *Bombyx mori* fibre (FSG) and *Nephila madagascarensis* spider fibre (SAM).

However, these fibres exhibit a less complex microstructure than keratin ones, high length (up to 1500–2000 m) and high optical quality. They can be considered as models for all fibrous proteins such as those constituting ligaments, artery walls etc. Classification is made from the stress (or load) versus strain curve, without considering their maximum values of stress and strain:

- Type I exhibits a linear elastic behaviour up to ∼2% (4% in keratin) of strain and then a quasi plateau is observed. A periodic variation of structure or residual stress is also observed along the fibre, likely in relation to the specific 8 motions made by the worm in making its cocoon.
- Type II consists of two-step linear elastic behaviours up to 5–6% with kinks at ∼2 and 5–6%, and then shows a quasi plateau.
- Type III is characterized by a smooth transition from a linear behaviour to a quasi plateau.
- Type IV starts rather similarly to type I but above ∼8–12% a quasi-linear 2nd behaviour is observed.
- Type V, the fibres break during the first elastic stage.

As shown in figure 5(a), the highest ultimate stresses were obtained for type I (fresh) non-degummed fibre and for type II or IV fibres. The plateau arises from the untwisting–lengthening of the helix (so call α-helix-β-sheet transition). The highest ultimate strains were often measured for the type IV fibres. Figure 5(a) exemplifies the different type observed for fresh *Bombyx mori* fibres. However, statistical data were established for hundreds of fibres of different origins: silkworms and spider silk and keratin fibres [16] (figure 5(b)). Unambiguously, type IV is obtained for sericin-free, dried or old fibres, Type III is characteristic of fibres saturated with water. Type II is more frequent for gummed fibres. Type V behaviour is only detected for heavy chemically- (acid/base or dyed degummed fibres) or thermally treated samples, i.e. after some chemical degradation.

4. Differentiating the 'crystalline'/'amorphous' conformations

4.1. Spectroscopic probes of the polymer conformation/structure

X–H vibrators (X=O or N) are considered as isolated vibrators because of the large mass difference between X and H atoms. Furthermore, the very anharmonic character of the X–H bond potential due to the H-bonding makes the stretching mode wavenumber and bandwidth very sensitive to the local structure [17]. Reliable curves between the wavenumber and the X–H…Y distance have long been established [32, 33]. However, the intrinsic mode width (resulting from the structural disorder alone, without mechanical coupling) is obtained only in the case of an isotopic dilution [H]/[D] <10%: very light vibrators normally couple in a complex way (mechanical, electric, quantum) with the other phonons and only with isotopic dilution, by removing the essence of these couplings, it becomes possible to obtain a spectrum giving details on the vibrators' environment [11, 34].

As an example, figure 6(a) compares the infrared signature of the PA66 fibre in its hydrogenated and deuterated forms: some modes shift according to the D/H mass effect [5] but the prominent change is the decrease of the bandwidth. When the H/D mole ratio is less than 10%, mechanical couplings are almost suppressed and the bandwidth of the X–H vibrator reflects the static and dynamic disorder [11]. In the case of PA66 fibre the N–H stretching mode appears made of two bands, a narrow one assigned to N–H vibrators in 'crystalline' environment and a broader one assigned to those in amorphous matrix [5]. Similar features are observed for Raman N–H fingerprint. The main component is the narrowest Raman peak at 3303 cm^{-1} ('Cr' bandwidth at half height ∼30 cm^{-1}, reduced to $L = 20\,cm^{-1}$ in diluted H/D isotopic polyamide fibre). The IR 'Cr' counterpart peaks at 3304 cm^{-1} (bandwidth ∼100 cm^{-1}, reduced to $L \sim 40\,cm^{-1}$ in diluted H/D isotopic polyamide fibre). These narrow peaks are well described with a Lorentzian function and can be assigned to 'crystalline' macromolecular chains.

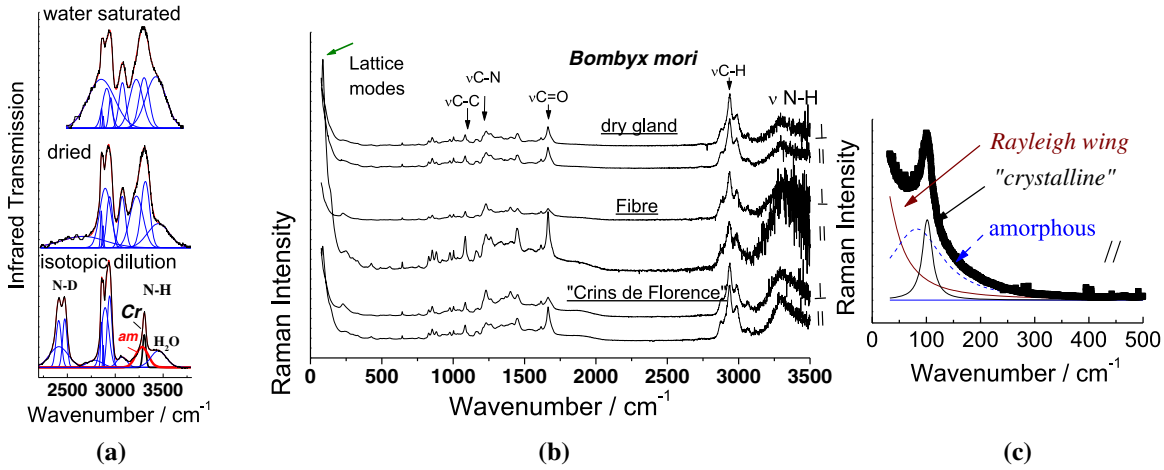

Figure 6. (a) Infrared transmission spectra of water saturated, dried and dried istotopic H/D diluted PA66 fibre. (b) Comparison of the Raman spectra recorded for *Bombyx mori* dried gland, degummed fibre and hand-spun '*Crins de Florence*'; note the high polarized vertical (‖) and perpendicular fibre spectra and the huge low wavenumber lattice mode peak, characteristic of the polyamide chain arrangement; (c) detail of the PA66 Raman low wavenumber spectrum and its components (see text).

The N–H wavenumber is insensitive to isotopic dilution and the peak corresponds well to a N–H vibrator almost free from any hydrogen bonds (dN–H $\cdots$ O $>$ 0.293 nm, see [33]). The much larger IR bandwidth results from the intrinsic larger broadness of IR modes due to the larger volume probed by the electric IR probe. In orthogonal polarization the intensity of this Lorentzian Raman component strongly decreases to the benefit of a broader Gaussian component (L, $\sim$80 cm^{-1}, figure 6(b)), ascribable to the 'amorphous' macromolecules. The higher wavenumber (G, 3310 cm^{-1}) indicates an absence of hydrogen bond, in agreement with a less compact structure. Two other weak bands are observed but it is difficult to know whether they both correspond to other types of N–H vibrators, or more probably to combinations, or result from a bad description of the line-shapes. The conservation of an amorphous component in V polarization confirms the isotropic character of the amorphous connections. Note that the re-hydrogenation of the deuterated fibres is slow and no remarkable difference between spectra carried out a few minutes after exiting the heavy water or 1 h afterwards is observed. The whole of these results confirms the existence of 'crystalline' and 'amorphous' or, rather, ordered and disordered conformation/structures of the macromolecular chains. The R/IR splitting being almost inexistent in the isotopically diluted state, it may be concluded that the local 'crystalline' and 'amorphous' structures in PA66 fibre are very similar and thus in agreement with a model of continuous angular disorder (para-crystal).

Actually, because of the very large intensity of the low wavenumber Raman external/lattice modes Raman analysis should be preferred (figures 6(a) and (b)). Figure 6(b) compares the signatures of silk raw material (spectra directly recorded on the *Bombyx mori* silkworm fibre, dry gland and hand-spun fibre from the gland). The spectral signatures of the amide group are systematically present, as observed for the PA66 fibre [7]. Assignments can be found in references [7, 8]. Figure 6(c) shows the low-frequency collective modes, the narrow one for 'ordered' polyamide chains and the broader for amorphous one. A large Rayleigh wing is also present due to the density heterogeneity at the subnanometric scale. The polarized Raman signatures have been normalized versus the C–H massif. The analysis agrees with the results of x-ray diffraction highlighting amorphous and more ordered 'crystalline' conformations and validates the choice to apply this description to the collective mode around 100 cm^{-1}. The fact that the νN–H wavenumber of the amorphous 'phase' is a little higher is in agreement with the lower energy of the corresponding chain collective mode, as observed in figure 6. The disappearance of the 'crystalline' component signature with polarization is nearly complete. Therefore, the analysis of the PA66 chain modes at $\sim$100 (crystalline)/80 (amorphous) cm^{-1} confirms the alignment of the crystalline macromolecular chains as well as the isotropic character of the amorphous phase. Similar features are observed for PET fibres, but a higher number of components can be distinguished in accordance with the higher crystallinity and lower symmetry of this compound [12].

For silks, this character is less marked and variable, according to the type of silk considered and the 'crystalline' collective mode measured at $\sim$80 cm^{-1} instead 100 cm^{-1} in PA66 fibre.

4.2. Tensile fibre behaviour under controlled strain/load

Raman shift as a probe of the (residual/applied) stress/strain was first developed for carbon fibre and C-fibre reinforced composite material because of the strong Raman signal of carbon and its resonance character. However, it is possible to easily measure the second harmonic spectrum ($1350/1600 \times 3$ cm^{-1} $\sim$ $4000/4800$ cm^{-1}) that multiplies by three times the sensitivity of the methods [21, 35–37]. The stress-induced Raman shift does not only depend on the stress but also—and mainly—on the bond anharmonicity [3, 36]. Anharmonicity is great for aromatic and hydrogen-bonded bonds. Note the Raman shift originating from temperature change is much larger than the stress-induced shift, thus a careful control of the temperature—i.e., use of low laser illumination power—is mandatory [36–38].

We will now address the collective low wavenumber signature of 'amorphous' and 'crystalline' polymer chains to

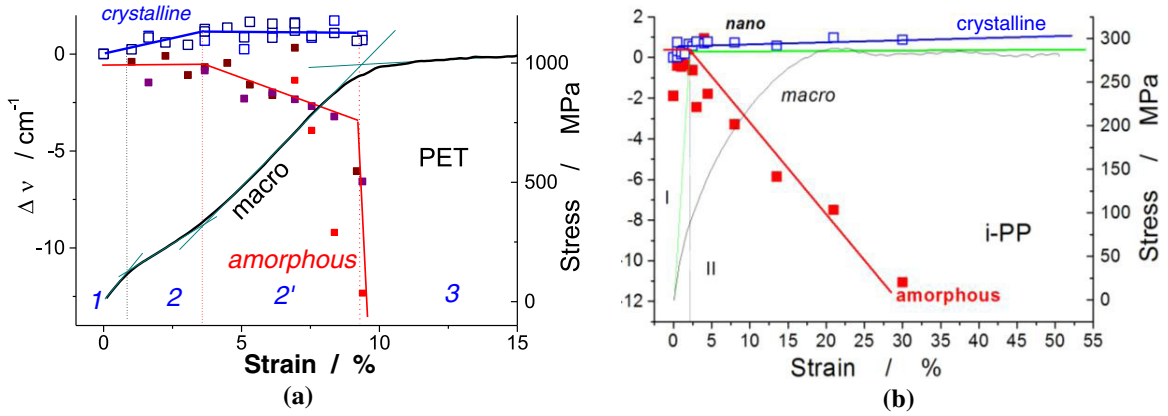

Figure 7. Comparison between the macroscopic tensile behaviour of (a) PET and (b) i-PP single fibre (black curve, left scale) and the nanomechanic behaviour of amorphous (blue open squares) and 'crystalline' (solid red square) macromolecular chains determined by the Raman lattice modes wavenumber shift. Given data correspond to 3–5 fibres.

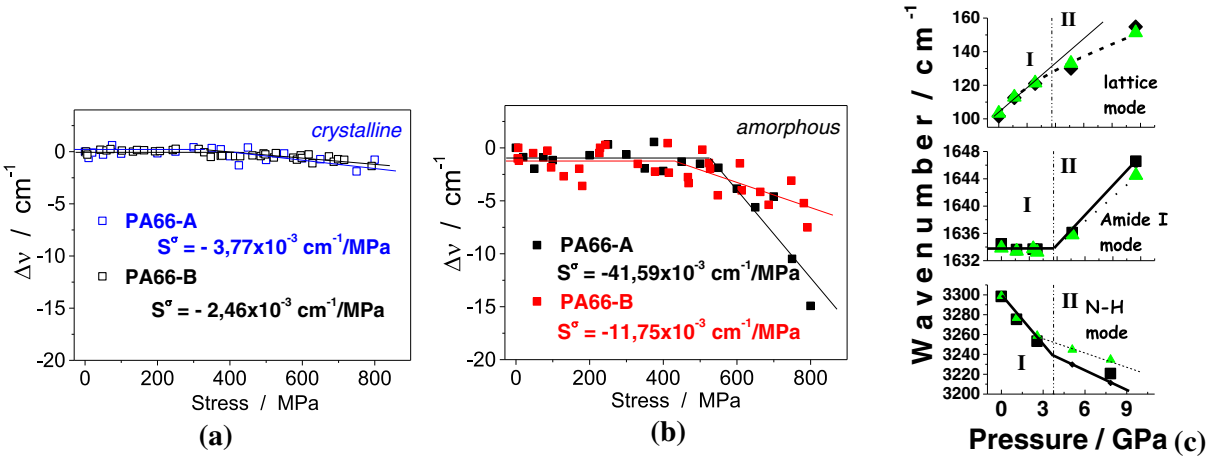

Figure 8. Raman wavenumber shift: comparison between the nanomechanic tensile behaviour of two PA66 single fibres produced by two different companies having similar ultimate strength but different fatigue behaviours. The nanomechanical behaviour of 'crystalline' ((a), open squares) and 'amorphous' ((b), solid squares) macromolecular chains determined from the Raman lattice modes wavenumber shift are compared: note the different slope rates in (b). (c) Evolution of the three characteristic Raman probes of PA66 in a diamond anvil cell.

understand the mechanical tensile and compressive behaviour with the examples of PA66 (90 and 100 cm^{-1}), PET (60 and 75 cm^{-1}) and i-PP (50 and 110 cm^{-1}) [12–18]. For keratin fibres, it was not possible to extract the low wavenumber components and we had to use the Amide I ($\nu C = O$), the N–H stretching and the S–S bridge modes [14].

We will first consider the stronger narrow (crystalline) and broad (amorphous) component of PET fibre spectra (figure 7(a)). This shows an initially viscoplastic behaviour until 450–500 MPa (~10–12% of lengthening), slightly varying according to the fibre producer. The amorphous bonds first and the crystalline ones later, are put into an increasingly rigid elastic tension (figure 7 [12]). The thresholds measured on the scale of the molecular bonds correspond to the transitions on the macroscopic stress–strain curve measured on single fibre between an initial softening, a pseudo-elastic regime and a nonlinear pre-rupture. This behaviour is very similar to that of a composite material with initial loading of the matrix alone (the amorphous matter), then that of the reinforcement (continuous ordered macromolecular chains) and the matrix simultaneously and, eventually, the degradation of the matrix followed by that of the reinforcement. The slight upward Raman shift measured for the crystalline signature indicates a Poisson's effect; the squeezing of the fibre diameter involved by the tensile stress compresses the crystalline islands, as sketched in the Oudet's model (figure 6(c) [39]). A very similar behaviour is measured for polypropylene but the downward shift starts at a low stress level in accordance with the high viscoelasticity of the material.

A very different behaviour is observed for PA66 fibre (figure 8): the Raman shift measured for crystalline and amorphous signatures is rather similar. This is consistent with the Prevorsek's model [40], in which a macromolecular chain belongs both to amorphous and to 'crystalline' regions (figure 6(b)). We observe a plateau up to ~500 MPa, i.e. up to the inflexion point of the macroscopic tensile stress–strain curve (figure 1(a)) and then a down slope, more or less pronounced as a function of the PA66 fibre producer. Changes are more significant for the amorphous component, as already observed for other fibres (figure 7). Actually, figure 8 compares data of two types of PA66 fibres, with very similar ultimate fracture strengths but produced by two different companies (their behaviour under fatigue

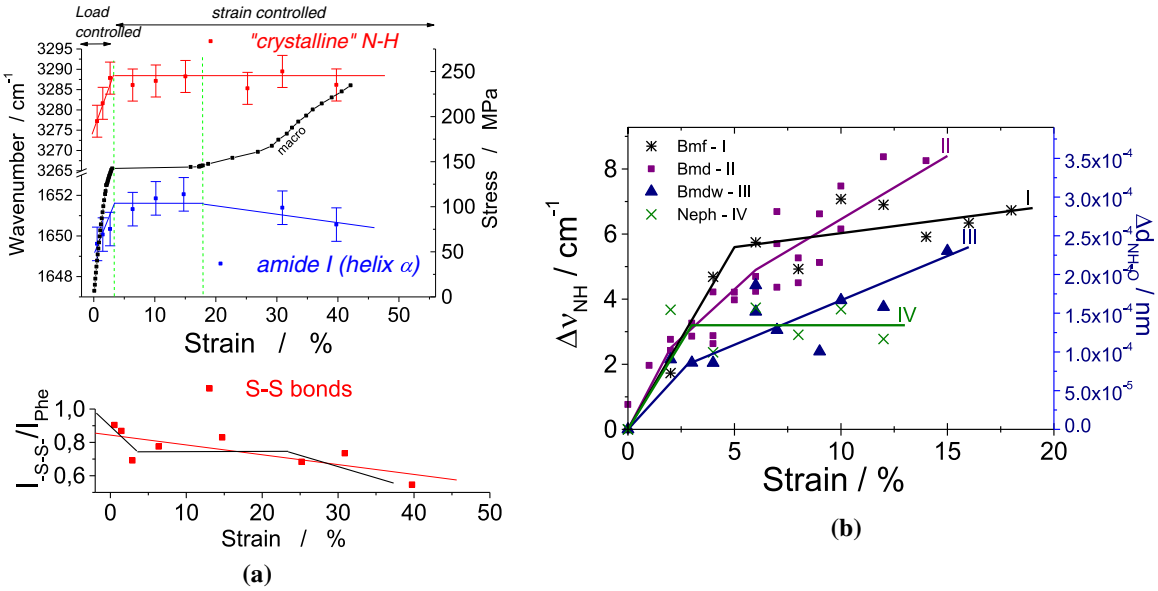

Figure 9. (a) Top, comparison between the nanomechanic tensile behaviour of a hair single fibre (black squares, right scale) with the Raman wavenumber plots of N–H and Amide I stretching modes; bottom, plot of the S–S bond mode normalized versus the phenyl ring one as a function of the applied strain. (b) Raman νN–H wavenumber shift measured for the different stress–strain behaviour types (see figure 5(a)).

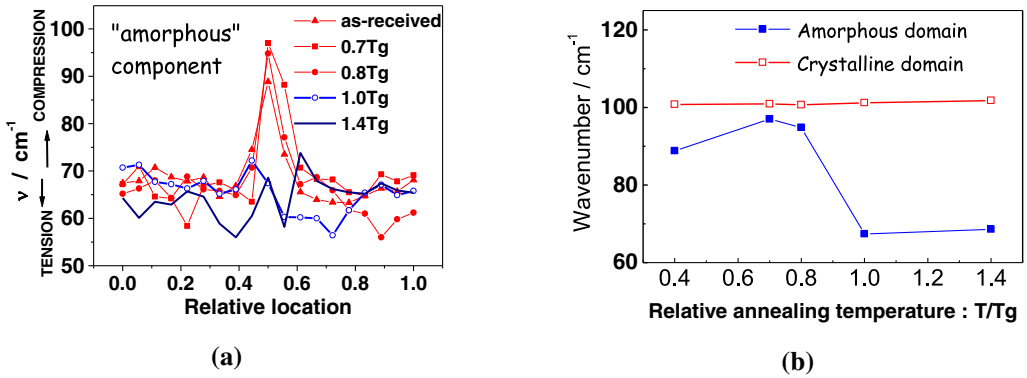

Figure 10. (a) Comparison of the Raman (amorphous) lattice mode wavenumber shift measured across the diameter of an as-received PA66 single fibre and after different thermal annealing below and above the glass transition temperature (T_g); (b) Comparison of the amorphous and 'crystalline' peak wavenumber as a function of annealing temperature versus glass transition one.

is different). No significant difference is measured for the crystalline component but the slopes of the 'amorphous' chain signal are different above the ~500 MPa threshold, indicating different behaviours in amorphous environment.

Figure 9(a) compares the macroscopic tensile stress–strain curve and the Raman wavenumber shift of N–H (~3277 cm^{-1}) and Amide I (~1650 cm^{-1}) bands of Caucasian white hair fibre. The relative intensity of the S–S bond (~510 cm^{-1}) versus strain is given in figure 9(a). A perfect relationship is observed between the macroscopic stress–strain behaviour and the nanoscopic Raman shift one: a linear elastic behaviour up to 4% of strain and then a plateau assigned to the α-helix opening transition allowing the possibility of a β-sheet arrangement. This transition is prepared by the breaking of S–S bonds (figure 9(a)).

The evolution of the Raman shift induced by controlled strain is shown in figure 9(b) for fibres exhibiting the characteristic types presented in figure 5(a). The behaviour measured at the nanometric scale by Raman scattering—the probe is the chemical bond polarizability—fits well with the macroscopic stress–strain behaviour.

4.3. Core/skin textures

The recording of a series of spectra across the fibre diameter (figure 3) with high magnification microscope objectives (spot diameter 5–1 μm) makes it possible to analyse the texture anisotropy of the various fibres. An example is given with PA66 fibre (figure 10) but measurements have also been conducted for PBO and PET [12] fibres and for silks [16–18]. A core–skin effect is obvious [12] from the wavenumber shift across the fibre diameter. These variations indicate a weak tension of the crystalline chains and a strong compression of the amorphous bonds in the fibre core.

The strong width reduction of the 'amorphous' macromolecular chain component in the fibre core undoubtedly indicates a much better organization, at the local scale, of the amorphous 'phase'. This characteristic can be related to the slower cooling of the fibre core.

Such anisotropy is consistent with a radial temperature gradient experimented by the fibre during the processing steps. A comparison of the data recorded for PA66 fibres thermally treated at various temperatures below and above

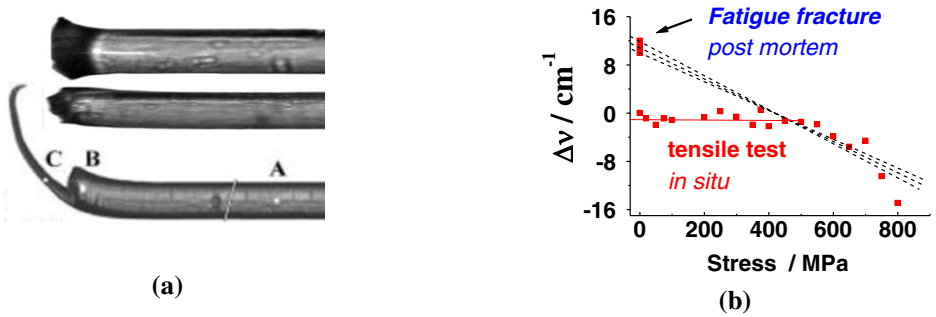

Figure 11. (a) Characteristic tips of cut (top) and fractured fibre by ultimate load (medium) and fatigue (bottom). (b) Comparison of the residual Raman shift (amorphous component) measured at the B–C points for fatigue fractured fibres with the behaviour measured for as-received single fibre up to their ultimate fracture [41].

the glass transition (T_g) temperature shows that the core/skin anisotropy disappears by annealing above T_g (figure 6), according to the above-proposed origin. The prominent role of a quenched skin layer in silicate glass to maximize the mechanical properties is well known in the glass industry. Different core/skin textures are observed as a function of fibre composition and producer.

4.4. Fatigue

Fatigue resistance studies, i.e. the solicitation of a material during a series of mechanical cycles between two load levels, one very low with respect to the ultimate strength (e.g. 5–10%) and the other not very far away from the ultimate value (e.g. 60–70%) are the most representative tests to design a material. The fatigue fracture mechanism is specific. This is illustrated by considering the habit of the fibre fracture, as shown in figure 11. A fracture performed by increasing the load up to the ultimate fracture gives a habit as visible in figure 3(a), a mirror-like surface in the area where the crack starts and then a more corrugated one. In contrast, a fatigue fracture shows an elongated tongue (figure 11(a)). The Raman analysis of fibres broken in fatigue along the line A–B–C highlighted a state of compressive stress of the amorphous phase close to the point of initiation of the rupture and its progressive decrease over 200–300 μm beyond this point [41]. As shown in figure 11(b) the upward shift measured in B–C points is located at the intersection between the y-axis and the slope of the 'amorphous' signal at a high level of strain. All occurs as if the rupture in fatigue resulted from the loss of viscoelasticity—and its characteristic plateau—at certain points, of the amorphous phase.

4.5. Compressive behaviour

Figure 8(c) compares the wavenumber shift of the low wavenumber lattice, Amide I and νN–H stretching modes of PA66 fibre in the diamond anvil cell (figure 4(d)). A threshold is observed at 4 GPa. Under hydrostatic pressure the coming together of the chain segments (reduction in νN–H wavenumber for both crystalline and amorphous chain conformation) can be clearly seen together with the existence of a threshold after which the geometry of the fibres is modified: the Amide I wavenumber, constant below 4 GPa, starts to shift and a slope change is observed for the low wavenumber mode. This confirms the higher sensitivity of N–H stretching and collective lattice mode with respect to the Amide I (or Amide III) modes, the bands used by other spectroscopy teams [42].

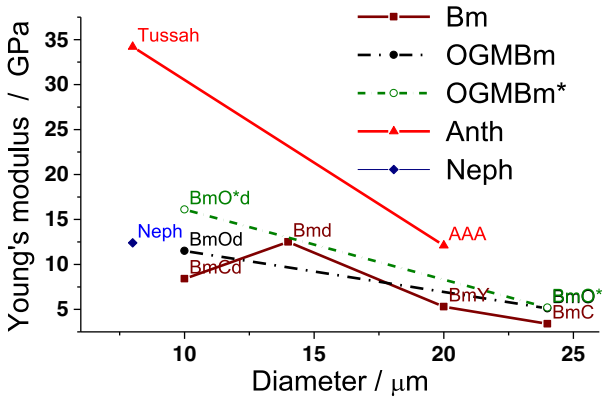

Figure 12. Evolution of the silk fibre Young's modulus as a function of the fibre diameter for different silks (*Tussah, Anthaerea, Bombyx mori* with or without genetic modification and *Nephila madagascarensis*).

5. Conclusion

The comparison of Young's modulus extracted from the stress–strain plots (figure 12), the most used characteristics to detect structural modifications from the mechanical analysis appears very sensitive to the object size and demonstrates the difficulty to compare material without complementary structural investigation. The combination of vibrational spectroscopy and stress–strain analysis offers new tools to study the structure changes as well as the mechanical behaviour. The possibility of separately analysing 'crystalline' and 'amorphous' macromolecule conformation/structure allows a new comprehension of the processes of fracture and fatigue at the different scales of the material. The key role of the bonds of amorphous macromolecular chains is confirmed, whereas hydrogen bonds seem too weak to influence the mechanics of the system. The comparison between natural and synthetic fibres shows that this study could be generalized.

Acknowledgments

The authors warmly thank Dr A Bunsell, Dr G Chavancy, Dr A Marcellan, Dr J M Herrera Ramirez, Dr R Paquin, Dr G

Gouadec, Dr A Percot and Dr H M Dinh for their contribution to this work.

References

[1] Michel J-M 2009 *Contribution to the History of the Polymer Industry in France (Contribution à l'Histoire Industrielle des Polymères en France)* (Paris: Société Chimique de France) http://www.societechimiquedefrance.fr/fr/documentations-scientifiques/contribution-a-l-histoire-industrielle-des-polymeres-en-france-par-jean-marie-michel/ (accessed October 2012)

[2] Bunsell AR and Schwartz P 2009 *Handbook of Tensile Properties of Textiles and Technical Fibres* (Oxford: Woodhead CRC)

[3] Gouadec G and Colomban Ph 2007 *Prog. Cryst. Growth Charact. Mater.* **53** 1

[4] Colomban Ph 2009 *Comput. Sci. Technol.* **69** 1437

[5] Colomban Ph and Gouadec G 2009 *Comput. Sci. Technol.* **69** 10

[6] Guinier A 1956 *Théorie et Technique de la Radiocristallographie* (Paris: Dunod)

[7] Marcellan A, Bunsell AR, Piques R and Colomban Ph 2003 *J. Mater. Sci.* **38** 2117

[8] Colomban Ph, Dinh HM, Riand J, Prinsloo L and Mauchamp B 2008 *J. Raman Spectrosc.* **39** 1749

[9] Colomban Ph, Folch S and Gruger A 1999 *Macromolecules* **32** 3080

[10] Mazerolles L, Folch S and Colomban Ph 1999 *Macromolecules* **32** 8504

[11] Pham Thi M, Colomban Ph and Novak A 1985 *J. Phys. Chem. Solids* **46** 493
Pham Thi M, Colomban Ph and Novak A 1985 *J. Phys. Chem. Solids* **46** 565

[12] Colomban Ph, Herrera Ramirez J M, Paquin R, Marcellan A and Bunsell A R 2006 *Eng. Fract. Mech.* **73** 2463

[13] Herrera Ramirez J M, Bunsell A R and Colomban Ph 2006 *J. Mater. Sci.* **41** 7261

[14] Paquin R and Colomban Ph 2007 *J. Raman Spectrosc.* **38** 504

[15] Colomban Ph, Aidi-Mounsi A and Limage M-H 2007 *J. Raman Spectrosc.* **38** 100

[16] Colomban Ph, Dinh H M, Bunsell A R and Mauchamp B 2012 *J. Raman Spectrosc.* **43** 425

[17] Colomban Ph and Dinh H M 2012 *J. Raman Spectrosc.* **43** 1035

[18] Colomban Ph, Tournié A, Dinh H M and Jauzein V 2012 *J. Raman Spectrosc.* **43** 1042

[19] Colomban Ph, Moukit S E, Dinh H M, Hassine M, Riand J and Mauchamp B 2008 *Rev. Comp. Mat. Avancés.* **18** 163

[20] Paquin R, Limage M-H and Colomban Ph 2007 *J. Raman Spectrosc.* **38** 1097

[21] Colomban Ph, Gouadec G, Mathez J, Tschiember J and Peres P 2006 Opaque *Compos.* Part A **37** 646

[22] Jauzein V and Colomban Ph 2009 Types, structure and mechanical properties of silk *Handbook of Tensile Properties of Textiles and Technical Fibres* ed A R Bunsell and P Schwartz (Oxford: Woodhead CRC) chapter 6, p 144

[23] Monti P, Taddei P, Freddi G, Asakura T and Tsukuda M 2001 *J. Raman Spectrosc.* **32** 103

[24] Purvis J and Bower DI 1976 *J. Polym. Sci. Polym. Phys.* B **14** 1461

[25] Bulkin B J, Lewin M and De Blasé M J 1985 *Macromolecules* **18** 2587

[26] Niss K, Begen B, Frick B, Ollivier J, Beraud A, Sokolov A, Novikov V N and Alba-Simionesco 2007 *Phys. Rev. Lett.* **99** 055502

[27] Caponi S, Corezzi S, Fioretto S, Fontana A, Monaco G and Rossi F 2009 *Phys. Rev. Lett.* **102** 027402

[28] Rossi B *et al* 2012 *J. Phys. Chem.* B **116** 5323

[29] Colomban Ph, Sagon G, Lesage M and Herrera Ramirez J M 2005 *Vib. Spectrosc.* **37** 83

[30] Dinh H M, Percot A and Colomban Ph *ICNP 2010: 2nd Int. Conf. on Natural Polymers, Bio-Polymers, Bio-Materials, their Composites, Blends, IPNs, Polyelectrolytes and Gels: Macro to Nano Scales (Kottayam, Kerala, India*, September 24–26 2010)

[31] Vollrath F and Knight DP 2001 *Nature* **410** 541

[32] Novak A 1974 *Struct. Bond.* **18** 177

[33] Colomban Ph, Gruger A, Novak A and Regis A 1994 *J. Mol. Struct.* **317** 261

[34] Colomban Ph (ed) 1992 *Proton Conductors* (Cambridge: Cambridge University Press)

[35] Young R J 1996 *J. Microsc.* **185** 199

[36] Colomban Ph 2002 *Adv. Eng. Mater.* **4** 535

[37] Gouadec G, Forgerit J-P and Colomban Ph 2002 2D Correlation *Comput. Sci. Technol.* **62** 505

[38] Gouadec G, Colomban Ph and Bansal NP 2001 *J. Am. Ceram. Soc.* **84** 1136

[39] Oudet C 1994 *Polymères, Structures et Propriétés* (Paris: Masson)

[40] Prevorsek D C, Harget P J and Sharma R K 1973 *J. Macromol. Sci.* B **8** 127

[41] Herrera Ramirez J M, Colomban Ph and Bunsell AR 2004 *J. Raman Spectrosc.* **35** 1063

[42] Rousseau M E, Beaulieu L, Lefèvre T, Parais J, Asakura T and Pezolet M 2006 *Biomacromolecules* **7** 2512